Incorporation of a ferrocene unit in the π-conjugated structure of donor-linker-acceptor (D-π-A) chromophores for nonlinear optics (NLO)

Raphaël J. Durand,[a] Sylvain Achelle,*[a] Sébastien Gauthier,*[a] Nolwenn Cabon,[a] Maxime Ducamp,[a] Samia Kahlal,[a] Jean-Yves Saillard,[a] Alberto Barsella,[b] and Françoise Robin-Le Guen[a]

[a] Univ. Rennes, CNRS, ISCR (Institut des Sciences Chimiques de Rennes) - UMR 6226, F-35000 Rennes, France. E-mails: sebastien.gauthier@univ-rennes1.fr, sylvain.achelle@univ-rennes1.fr, Tel:+33 2 96 46 93 44, +33 2 96 46 94 48

[b] Département d'Optique ultrarapide et Nanophotonique, IPCMS, UMR CNRS 7504, Université de Strasbourg, 23 rue du Loess, BP 43, 67034 Strasbourg Cedex 2, France.

Abstract

In this paper we describe the synthesis, the electrochemical behaviour as well as the linear and nonlinear optical (NLO) properties of two push-pull derivatives bearing pyranylidene electron donating fragment, pyrimidine/methyl pyrimidinium electron withdrawing moiety and a ferrocene part in the π-conjugated bridge. The properties of these two compounds were compared to their analogues without ferrocene or pyranylidene fragments. Experimental results were completed with DFT calculations to gain further insight into the intramolecular charge transfer (ICT). All the results indicate a significant charge transfer through the ferrocene unit. The ICT is however more limited than in all organic analogues.

1. Introduction

The development of organic and organometallic second order nonlinear optical (NLO) chromophores has been an intensive research subject due to their potential in key field such as photonic[1–4] and electro-optics.[5–9] Key applications of second order NLO chromophores

include optical signal processing, integrated optics and second harmonic generation (SHG) microscopy. In comparison with inorganic NLO crystals such as lithium niobate, organic or organometallic NLO chromophores have many advantages such as a lower cost, larger and faster NLO responses.[10–12]

Second order NLO properties require the absence of centrosymmetry and generally the second order NLO chromophores are based on an electron-donating group (D) and an electron-withdrawing group (A) linked by a π-conjugated bridge (D-π-A).[10–15] NLO properties are directly related to the intramolecular charge transfer (ICT) occurring in such structures and can be easily tuned by varying the nature of the donor/acceptor couple and the π-conjugated spacer.[16–18]

In our group, we have recently optimized the NLO properties of chromophores based on pyrimidine[19–24] and/or pyranylidene[22–27] moieties as electron-withdrawing and electron-donating fragments respectively. It has been shown that pyrimidine and methylated pyrimidinium salts exhibit higher electron-withdrawing character than well-known pyridine analogues.[28] Proaromatic pyranylidene moieties, capable of gaining aromaticity upon ICT process into the push-pull structure, are now well-established electron-donating groups.[25,29–32] The ferrocene moiety has been extensively used as electron-donating part of NLO chromophores.[13,33–37] Ferrocene exhibits a good thermal and photochemical stability and the possibility of redox switching at low redox potential.[38,39] Ferrocene has rarely been used as spacer between donor and acceptor parts of push-pull molecules even if electron-transfer through the ferrocene has been demonstrated.[40–42] In this case, the charge transfer occurs "through space" and represents an alternative molecular strategy for NLO chromophores.[43,44] 1,1'-disubstituted ferrocenes with aromatic or alkynyl substituents generally adopt a stacked *syn*-conformation due to the electronic preference of the ferrocene and favorable π-π

interactions.[40,45,46] However, it has been shown that the introduction of charges to the ferrocene substituents can induce rotation to the *anti*-conformation.[47,48]

In continuation of our work regarding the incorporation of metal centers in the π-conjugated core of push-pull chromophores,[23,24] in this contribution we describe the synthesis, electrochemical, photophysical and second order NLO properties of two chromophores **1** and **2** with the following structure: D-π-Fc-π-A (Chart 1). In order to study the influence of the ferrocene units, the properties of these compounds will be compared with their D-π-A organic analogues **3** and **4** and Fc-π-A chromophores **5** and **6** in which the ferrocene plays the role of electron-donating group.

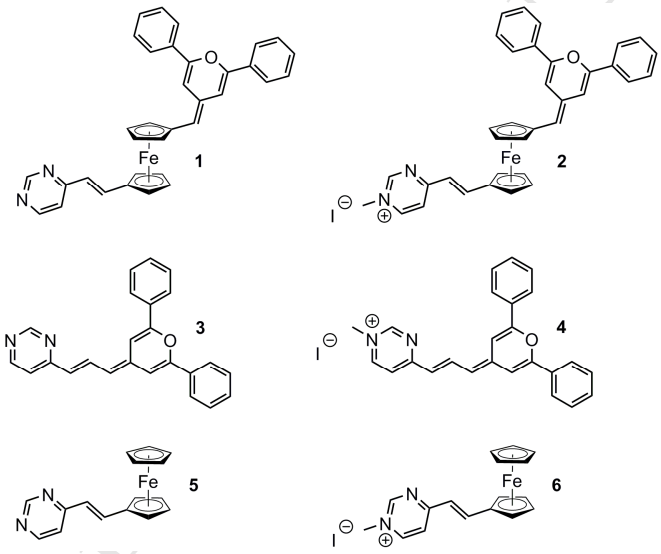

Chart. 1

2. Results and discussion

2.1. Synthesis

The asymmetrical ferrocene complex **1** was obtained in two steps. A Wittig reaction was first carried out with stoichiometric amounts of 1,1'-ferrocenedicarboxaldehyde and pyranylidene phosphonium salt[49] to give compound **7**.**50** The second carbonyl group reacted with 4-methylpyrimidine through a Knoevenagel condensation to form a *trans*-alkene, according to a procedure already described[19] (Scheme 1). The compounds **1**, **3**[51] and **5**[19] could easily be

methylated under reflux with iodomethane in pyrimidinium iodide to give complexes **2**, **4** and **6** respectively in excellent yields (>95%) (Scheme 2). This *N*-methylation occurs regioselectively on the nitrogen in position 1 of the heterocyclic ring.[20]

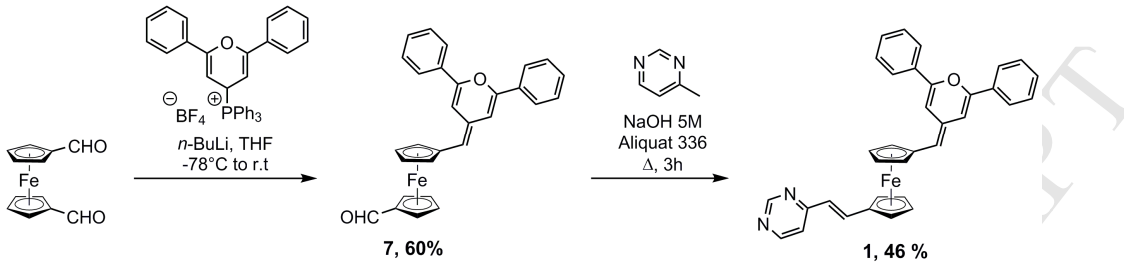

Scheme 1 Synthesis of compound **1**

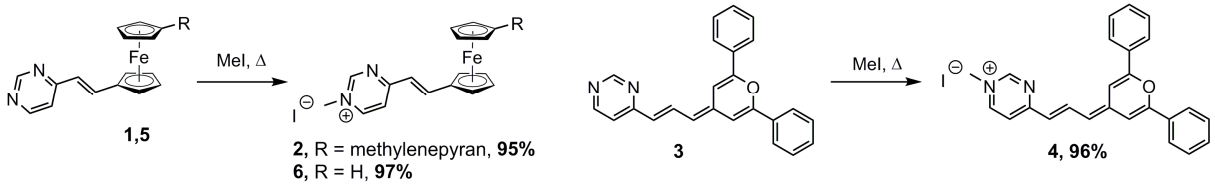

Scheme 2 Synthesis of *N*-methylpyrimidinium derivatives **2**, **4** and **6**

The compounds **1–6** were characterized by IR, NMR (^{1}H, and ^{13}C) and high-resolution mass spectrometry. These characterization data fully support the proposed structures. The ^{1}H NMR spectrum of **1** displays signals for the pyranylidene ligand (two vinylic H resonances of the methylenepyran core appearing as two doublets at δ = 6.73 and 6.09 ppm, $^4J_{HH}$ = 1.4 Hz), the exocyclic H of the methylenepyran moiety at δ = 5.34 ppm, the diazine ring (δ = 8.88 and 8.26 ppm), the *trans*-double bond (two doublets at δ = 6.51 and 7.57 ppm, $^3J_{HH}$ = 15.8 Hz), the two cyclopentadienyl fragments of the ferrocene (δ = 4.53, 4.42, 4.40, 4.26 ppm) and the aromatic protons. The singlet signal for the methyl group located on the pyrimidine ring (*e.g.* for **2**: δ = 3.47 ppm in ^{1}H NMR and δ = 44.4 ppm in ^{13}C NMR) clearly appears on compounds **2**, **4** and **6** spectra.

2.2. Electrochemical studies

Electrochemical studies were performed in order to examine redox potentials of the compounds **1**-**6** and to compare the energy band gap ΔE of this series of compound ($\Delta E = E^{ox} - E^{red}$). Cyclic voltammetric (CV) studies of compounds **1**–**6** were carried out with a carbon working electrode in dry N_2-purged CH_2Cl_2 containing 0.1 M $[Bu_4N][PF_6]$ as supporting electrolyte. All potentials are given *vs* $Me_{10}Fc$. Electrochemical data are gathered in Table 1 and led to the following points:

a) Cationic complexes **2**, **4** and **6** bearing the redox-active iodide counteranion I^- display an oxidation peak at around 0.5 V, which can be attributed to the oxidation of the iodide anion.[23]

b) Compounds **1**-**4** present cyclic voltammograms which are characteristic of the redox behaviors of pyranylidene-containing compounds.[27,51,52] Indeed for the ferrocenyl derivatives **1** and **2**, an irreversible anodic peak (at 0.40V and 0.51V respectively), which may involve the oxidation of the pyranylidene moiety into a radical cation, is observed on the forward scan. This latter immediately reacts by dimerization to form a bispyrylium salt,[52] which is detected on the backward scan at around -0.15 V (irreversible cathodic peak). This C-C bond making/breaking process upon electron transfer has been largely studied in our laboratory and allow us to do the assignment of these oxidation peaks to the oxidation of the pyranylidene fragment.[53] For **2**, this oxidation process take place at the same potential that the iodide oxidation. In the case of the organic compounds **3** and **4**, when an anodic scan is performed, no clear cathodic peak is detected on the reverse cathodic scan, probably because several C-C coupling processes may occur in the extended π-system.[51] However, for

compound **3** the oxidation peak at 0.62 V can be attributed to the oxidation of the pyranylidene fragment.

In addition, for **1,** the two reversible systems, at 0.70V and 0.83V can be attributed to the ferrocenyl groups of the bispyrylium compound formed during the oxidation process.[52] In the case of **2**, these systems are badly defined because of a deposition phenomenon at the electrode surface.

c) For neutral compounds **1**, **3** and **5**, the pyrimidine moiety is reduced at -1.83, -1.48 and -1.86 V respectively. This reflects a better electronic delocalization in the compound **3**. Concerning the oxidation process, Oxidation at a slightly lower potential is observed for **1** *vs* **5** in regard to the electron donating effect of the methylenepyran fragment on the ferrocenyl group.

d) *N*-methylated pyrimidinium compounds **2**, **4** and **6** present a cathodic peak E_p^{red1} at -0.78, -0.65 ($E_{1/2}^{red1}$) and -0.74 V respectively on the cyclic voltammogram. This reduction may involve mainly the reduction of the pyrimidinium acceptor moiety.

The aforementioned elements led us to the two following suggestions:

i) Among the three neutral compounds, the lowest energetic gap ΔE ($\Delta E = E^{ox} - E^{red}$) is calculated for the organic compound **3** (2.12 V) *vs* the ferrocenyl derivatives **1** (2.23 V) and **5** (2.48 V); which is in favour of a better electronic delocalization for the organic derivative **3** (**3**>**1**>**5**);

ii) Due to the enhanced withdrawing effect of the pyrimidinium fragment, the reduction peak E_p^{red1} of the methylated complexes **2**, **4** and is significantly lowered (0.83 to 1.12 V) compared to the neutral precursor **1**, **3** and **5** respectively. By

consequence the band gap ΔE must be lowered and a better ICT is expected in this cationic series.

Table 1 CV data for compounds **1**–**6** in CH_2Cl_2/[*n*-Bu_4N][BF_4] (0.1 M), v = 0.1 V s^{-1}, *E*/V *vs.* $Me_{10}Fc$, Carbon disk working electrode.

Compound	E_p^{ox1}	$E_{1/2}^{ox2}$	$E_{1/2}^{ox3}$	E_p^{red1}	E_p^{red2}
1	0.40	0.70	0.83	-1.83	
2	0.51	0.66[a]	0.92[a]	-0.78	
3	0.64	–	–	-1.48[b]	
4	0.53	0.85[c]	–	-0.65[b]	-1.51
5	0.62[c]	–	–	-1.86	–
6	0.51	0.60	–	-0.74	-1.74

[a] *badly defined reverse peak: E_p is given instead of $E_{1/2}$;* [b] *quasi-reversible peak, $E_{1/2}$ is given instead of $E_{p;}$* [c] *irreversible peak: E_p is given instead of $E_{1/2}$*

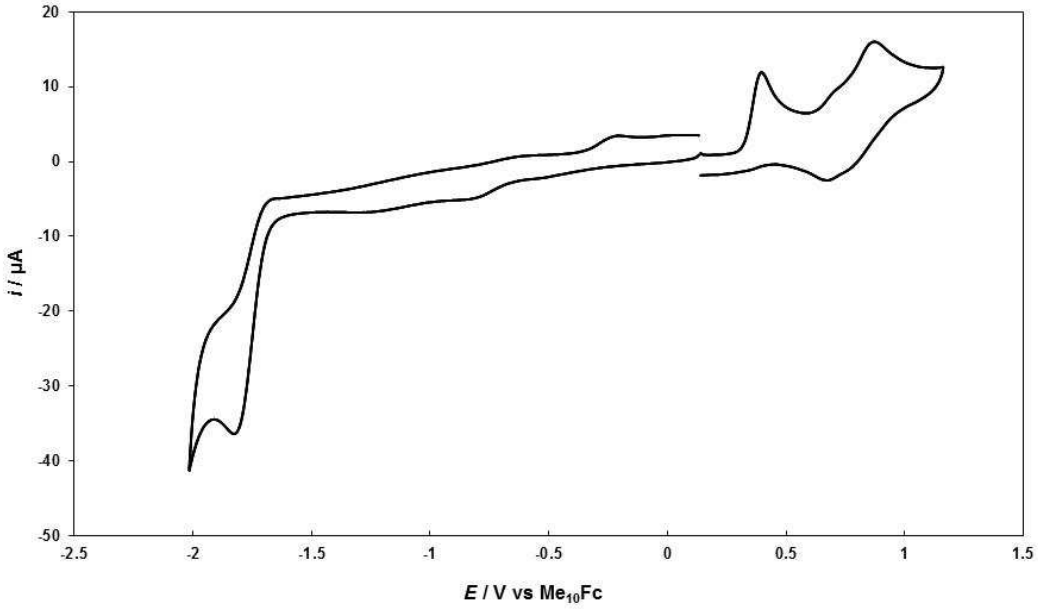

Figure 1 Cyclic voltammogram of **1** (C = 1.3 10^{-3} M in CH_2Cl_2/[*n*-Bu_4N][BF_4] (0.1 M), Carbon working electrode, *E*/V *vs.* $Me_{10}Fc$, v = 0.1 V s^{-1})

2.3. UV-vis spectroscopy

The absorption spectra of compounds **1**–**6** (Figure 1) were recorded in chloroform at a concentration of 10^{-3}–10^{-4} M in the 270–800 nm wavelength range and the results are given in Table 2. For ferrocene derivatives **1**, **2**, **5** and **6**, the lower energy bands (λ = 512, 684, 489 and 626 nm respectively), can probably be assigned to the metal-to-ligand charge transfer transition (MLCT).[33,54] The higher wavelength bands for organic compounds **3** and **4** and the second higher wavelength bands for complexes **1**, **2**, **5**, and **6** represent ICT between donor and acceptor parts. These ICT bands are in the wavelength range of 370 – 630 nm. For compound **2**, the ICT transition corresponds to the shoulder observed around 420 nm. The methylated compounds **2**, **4** and **6** exhibit red-shifted ICT band in comparison with their neutral analogues **1**, **3** and **5** respectively, indicating a better ICT. For neutral compounds **1**, **3** and **5**, it can be noticed that the organic push-pull molecule **3** exhibits the most red-shifted ICT band at 452 nm, whereas the ICT bands of the ferrocene derivatives **1** and **5** are similar. The same trend with the methylated complexes was observed: organic compound **4** exhibits the most red-shifted ICT absorption band (624 nm) but in this series compound **2** exhibits a significantly red-shifted ICT absorption band in comparison with **6**: the introduction of the pyranylidene fragment on the ferrocene unit significantly enhances the ICT.

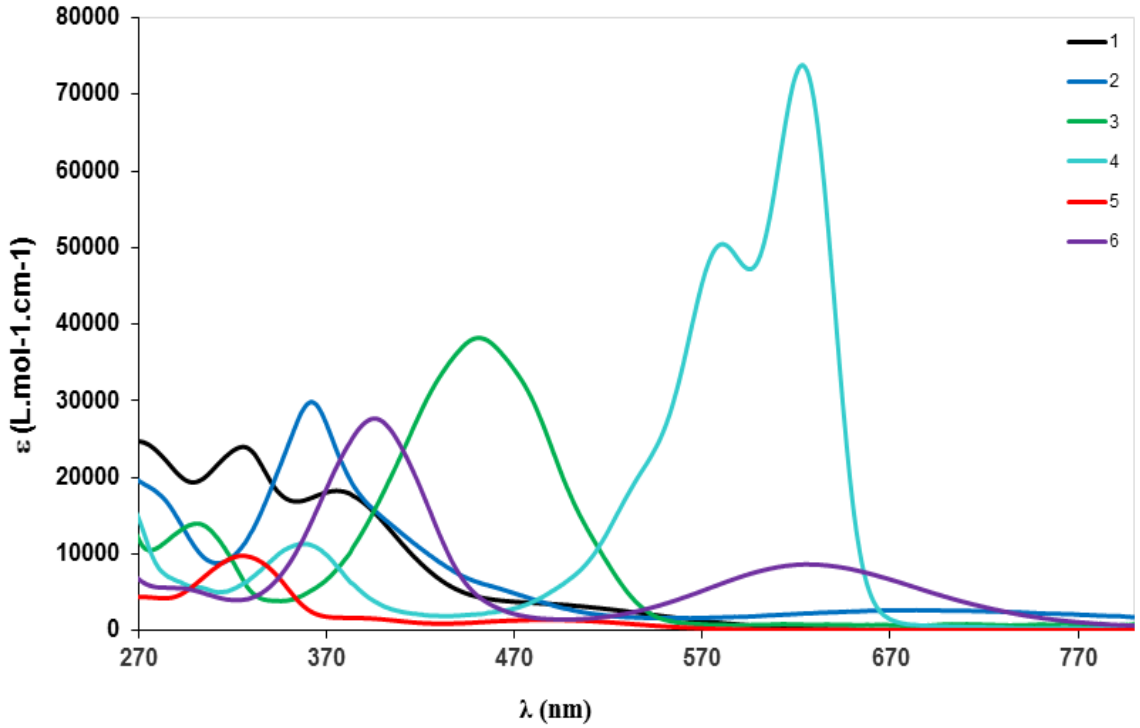

Figure 1 UV-Vis spectra of compounds **1–6** in $CHCl_3$

Table 2 Optical data of chromophores **1–6** in $CHCl_3$

Compound	λ_{max}[a] [nm] λ_{calc}[b] [nm]	λ_{max}[a] [nm]	ε[a] [mM^{-1} cm^{-1}]	$\mu\beta$[c] [10^{-48} esu]
1	326/376/512 299/351/568	326/376/512	24/18/3.0	60
2	362/420sh/684 346/ - /664	362/420sh/684	30/10/2.7	1320
3	301/452 276/430	301/452	14/38	310
4	360/581/624 332/504/ -	360/581/624	11/51/74	2220
5	326/384/489 306/ - /548	326/384/489	10/1.7/1.4	160
6	288/396/626 - / 370/578	288/396/626	5.6/28/8.7	<550[d]

[a] All spectra were recorded in $CHCl_3$ solutions at room temperature at c = 10^{-3} – 10^{-4} M in the 250 – 800 nm wavelength range. [d]TD-DFT calculated major transitions [c] $\mu\beta$ (2ω) measured by EFISH method at 1907 nm. Molecular concentration used for the measurements were in the range 10^{-3} to 10^{-2} M. $\mu\beta$ ± 10%. [d] No stable value was obtained

2.4. EFISH experiments

The second-order NLO responses of chromophores **1**-**6** were measured by the EFISH technique in $CHCl_3$ solution with a non resonant incident wavelength of 1907 nm. The second harmonic at λ = 953 nm stays well clear of the absorption bands of the chromophores. Experimental details on EFISH measurements are given elsewhere.[55] EFISH measurements provide information about the scalar product $\mu\beta$ (2ω) of the vector component of the first hyperpolarisability tensor β and the dipole moment vector.[56-59] This product is derived according to equation 1 and considering γ_0(-2ω,ω,ω,0), the third-order term, as negligible for the push-pull compounds under consideration. This approximation is usually used for push-pull organic and organometallic molecules.

$$\gamma_{EFISH} = \mu\beta/5kT + \gamma_0(-2\omega,\omega,\omega,0) \qquad \text{Eq. 1}$$

The results of EFISH measurements are presented in Table 2. For all the compounds, positive $\mu\beta$ were obtained, indicating that excited states are more polarized than the ground state and that both ground and excited states are polarized in the same direction. It should be noted that no stable $\mu\beta$ value was obtained for compound **6** that did not seem stable under EFISH measurement. As expected, pyrimidinium derivatives **2** and **4** exhibit higher NLO response than their neutral analogues **1** and **3**. Fully organic compounds **3** and **4** exhibit significantly higher NLO responses than ferrocene derivatives **1** and **2**. These results are in full accordance with the electrochemical and UV-visible data: the introduction of the ferrocene unit into the π-conjugated bridge lowers the ICT between the pyranylidene and the pyrimidine/pyrimidinium

fragments. Nevertheless, it should be noted that the NLO response observed for compound **2** ($\mu\beta$ = 1320 10^{-48} esu) is significantly than for **6** which tends to indicate ICT through the ferrocene fragment.

2.5. Computational investigation

Density functional theory (DFT) calculations have been performed on complexes **1** and **2**, as well as the closely related hypothetical derivatives **1'** and **2'** which have a phenyl substituent on the pyranylidene carbon situated in the α position with respect to Fc (see Scheme 3). Compounds **3-6** were also computed. The geometries were fully optimized at the PBE0-GD3BJ/Def2-TZVP level, solvent ($CHCl_3$) effect corrections included (see computational details). In the case of the push-pull complexes, two different conformers, *syn* and *anti*, were found, depending on the respective positions of the pyranylidene and pyrimidine chains. Interestingly, the *syn* isomer was found to be the most stable, by 3-4 kcal/mol in the case of **1** and **2** and 5-6 kcal/mol in the case of their substituted homologues **1'** and **2'** (Gibbs energy). In this conformation, the two ferrocenyl substituents are almost perfectly eclipsed (C_5/C_5 staggering angle lower than 2°), whereas the cyclopentadienyl rings remain almost perfectly parallel, making angles lower that 2°. The energy preference for the more crowded *syn* conformation is the consequence of significant non-covalent π-π interactions (dispersion forces). In the four computed complexes, the corresponding shortest C…C and C...O interplane contacts lie in the range 3.4-3.5 Å and 3.3-3.4 Å, respectively. The structures of both conformers with their relative energies are provided in Figure S1. The optimized geometries of complexes **1** (*syn*), **2** (*syn*), **5** and **6** are shown in Figure 3. Selected bond distances are given in Table 3, together with the computed HOMO-LUMO gaps, the trend of which is fully consistent with the electrochemical results. All of these findings suggest that the organic species are more conjugated than their organometallic counterparts

and methylated cations are more conjugated than their neutral relatives as noted previously for related metal complexes,[23-24]. Comparison of bond distances indicates the same trend and only small differences with respect to conjugation between the complexes. Our NBO charge analysis of the studied complexes is fully consistent with the above statements. In **1** the charges of the pyranylidene and pyrimidine branches are +0.06 and -0.02 respectively (-0.04 for the ferrocenyl unit), indicating a moderate charge transfer between the branches. For comparison, the charges of the same fragments in **3**, are +0.15 and -0.15, respectively, denoting larger charge transfer in the organic analogue. In the case of the methylated species **2** and **4**, the corresponding fragment charges are +0.07/+0.85 and +0.41/+0.59, indicating again a better electronic communication in the organic species, but also larger charge transfer in the methylated species as compared to their non-methylated neutral homologues. The presence of an additional phenyl substituent on the **1'** and **2'** models (Scheme 3) has little structural/electronic effect. It should be also mentioned that the high-energy *anti* conformers of the computed push-pull models exhibit rather similar distances and electronic structures than their *syn* counterparts. Similarly, their optical properties are similar and will not be discussed below.

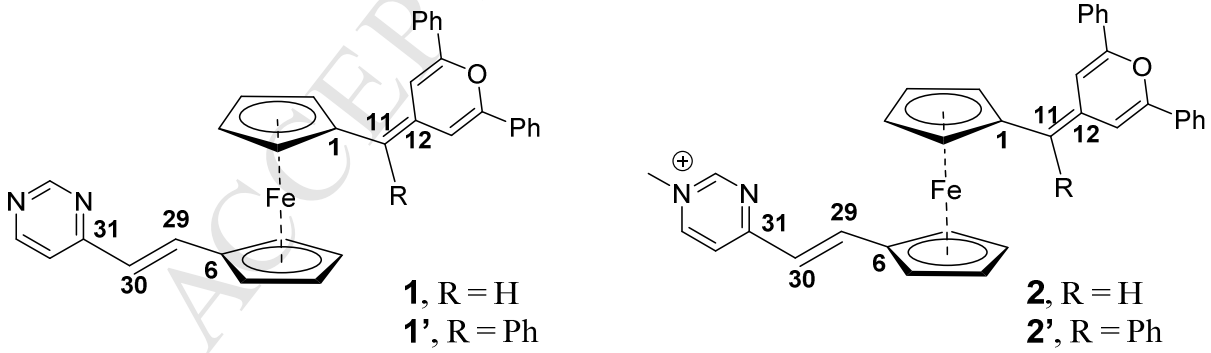

Scheme 3 The computed push-pull models with atom numbering used in the calculations. The atom numbering adopted for **5** and **6** is the same (when applying).

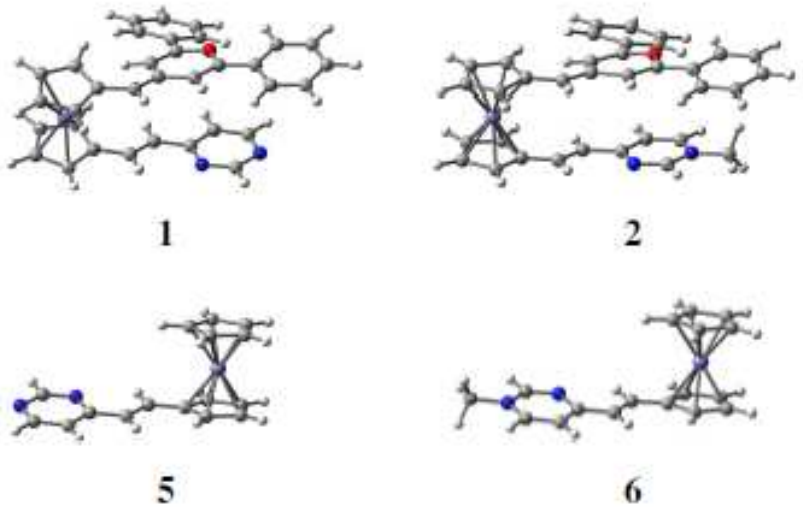

Figure 3 Optimized geometries of complexes **1** (*syn*), **2** (*syn*), **5** and **6.**

Table 3 Selected data (distances in Å) from the optimized geometries of chromophores **1**, **2**, **1'** and **2'** in their low-energy *syn* conformation, and compounds **3-6** (atom numbering according to Scheme 3).

Compound	**1**	**2**	**1'**	**2'**	**3**	**4**	**5**	**6**
HOMO-LUMO gap (eV)	5.47	4.27	5.30	4.13	3.12	2.79	6.48	5.37
$(Fe\text{-}C)_{av.}$	2.048	2.049	2.049	2.050			2.048	2.049
$[C(Cp)\text{-}C(Cp)]_{av.}$	1.390	1.390	1.390	1.390			1.422	1.422
C1-C11	1.448	1.445	1.463	1.462				
C11-C12	1.357	1.359	1.368	1.368	1.374	1.397		
C6-C29	1.442	1.425	1.443	1.426			1.445	1.427
C29-C30	1.339	1.354	1.339	1.353	1.356	1.382	1.341	1.357
C30-C31	1.451	1.421	1.450	1.421	1.442	1.382	1.453	1.424

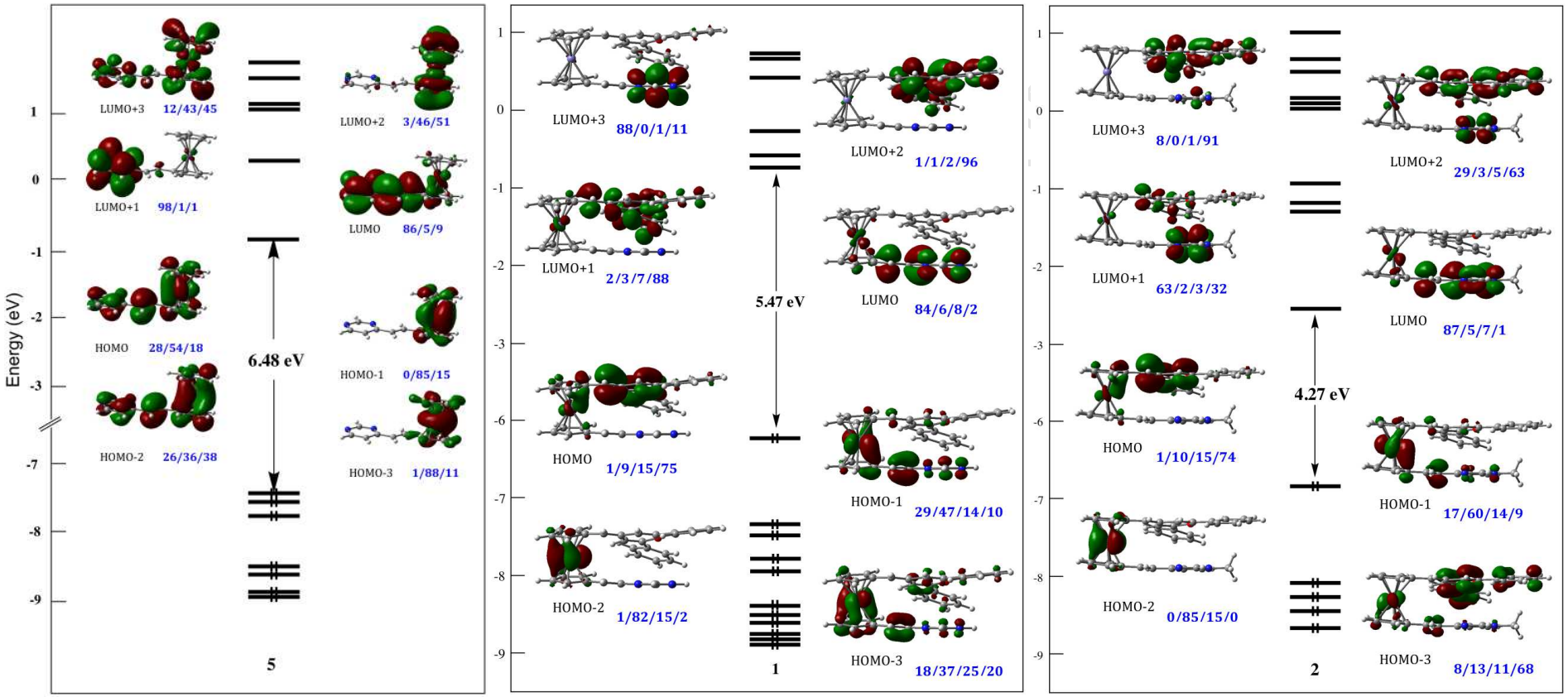

Figure 4 Kohn-Sham orbital diagrams of **5** (left), **1** (middle) and **2** (right). The numbers correspond to the following fragment contributions to the orbital localizations (%): The numbers correspond to the following fragment contributions to the orbital localizations (%): *Pyrimidine branch/Fe/cyclopentadienyls/pyranylidene branch*

The Kohn-Sham orbital diagrams of **5**, **1** and **2** are shown in Figure 4 for the sake of comparison. Whereas the highest occupied orbitals of **5** have substantial Fe character, the two lowest vacant orbitals have a large pyrimidine localization. The situation is different for **1** and **2** for which the HOMO and HOMO-1 are localized on the pyranylidene and pyrimidine sides, respectively. The situation is reversed for their LUMO and LUMO+1. Going from **1** to its methylated cation **2** tends to stabilize the pyrimidine-centered orbitals where the cationic charge is localized. As a consequence, the LUMO of **2** is lower than that of **1**, reducing substantially the HOMO-LUMO gap. For similar reason, the LUMO+3 of **1** becomes the LUMO+1 in **2**, with some minor pyranylidene admixture. The level orderings of **1'** and **2'** are similar to that of their **1** and **2** relatives.

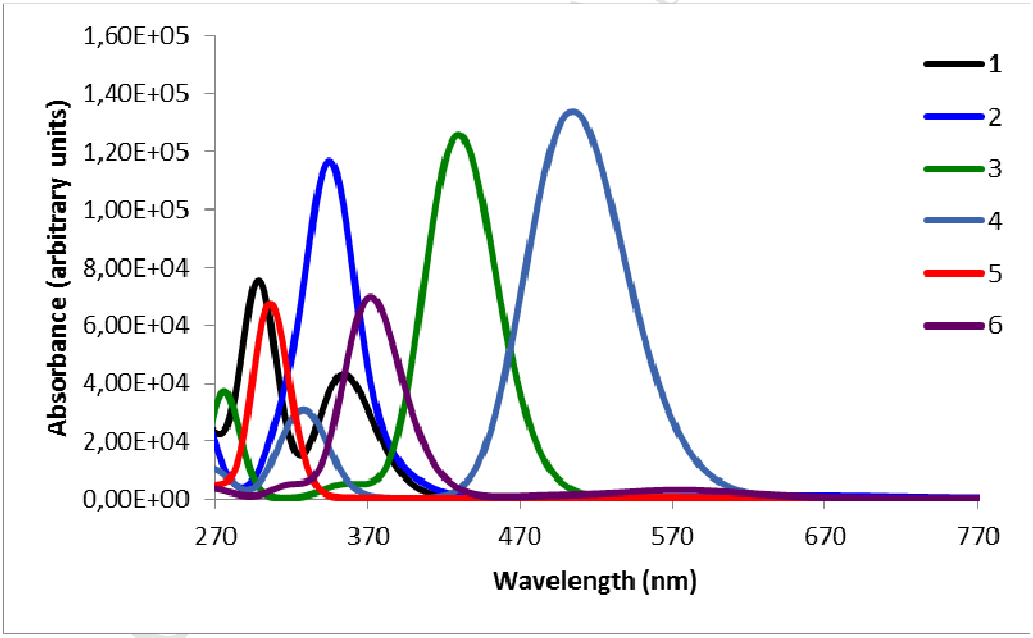

Figure 5 TD-DFT simulated spectra of compounds **1-6.**

The UV-vis excitation energies of complexes **1-6**, were computed by time-dependent DFT (TD-DFT) calculations at the CAM-B3LYP level (see Computational details). The major transitions energies are reported in Table 2, besides the corresponding experimental λ_{max} values, and the simulated spectra in Figure 5. There is a good agreement between the

simulated and recorded spectra. For all the computed compounds, the only transition associated with a large electron transfer (from pyranylidene to pyrimidine for **1**-**4** and from Fc to pyrimidine in the case of **5** and **6**) is that of higher energy, *i.e.* that corresponding to the band of larger intensity (Figure 5). Unsurprisingly, they are somewhat larger in the methylated cations, as compared to their neutral relatives.

Table 4 TD-DFT-computed hyperpolarizabilities for compounds **1-6** (in 10^{-30} esu).

Compound	**1**	**2**	**3**	**4**	**5**	**6**
β_{static}	20	52	71	94	22	76
$\beta_{dynamic}$ [a]	25	71	99	131	27	105

[a] computed at 1907 nm.

Quadratic non-linear optical hyperpolarizabilities have been also computed for compounds **1-6** (see computational details). The calculated β_{static} and $\beta_{dynamic}$ (at 1907 nm) values are given in Table 4. Although these results have to be considered only at a qualitative level, they are in a good agreement with the EFISH measurements (see above).

3. Conclusion

In summary, we have designed and prepared six push-pull chromophores to evaluate the effects of the ferrocene, the pyranylidene and the pyrimidine/ methyl pyrimidium fragments on the electrochemical, photophysical and NLO properties in D-π-A systems. The most effective NLO responses have been found with pyranylidene-*N*-methylated pyrimidine ring push–pull chromophores **2** and **4** incorporating or not the ferrocene moiety in the π-conjugated core. Spectroscopic, electrochemical and theoretical DFT studies of the compounds corroborated their suitability as nonlinear optical chromophores based on their opto-electronic properties. A significant ICT through the ferrocene unit has been

demonstrated by experimental and DFT studies but stays limited in comparison of all metal-free organic analogues. Nevertheless, we believe that the synthetic strategy developed in this study could open up new avenues for the design of novel ferrocene push-pull chromophores with more versatile opto-electronic properties and controllable molecular redox switches structures.

4. Experimental section

4.1. General Methods

All reactions were conducted under a dry nitrogen atmosphere using Schlenk techniques, but workups were carried out in air. The starting materials were purchased from Sigma-Aldrich or Alfa-Aesar and were used as received. The solvents were used as received except tetrahydrofuran that was distilled under a dry nitrogen atmosphere over sodium and benzophenone. Compounds **3**[51] and **5**[19] were obtained according to reported procedures. NMR spectra were acquired at room temperature on a Bruker AC-300 spectrometer (^{1}H at 300 MHz, ^{13}C at 75 MHz) and referenced as follows: ^{1}H NMR, residual $CHCl_3$ (δ = 7.26 ppm); $^{13}C\{^{1}H\}$ NMR, internal $CDCl_3$ (δ = 77.16 ppm). The chemical shifts δ are reported in parts per million relative to TMS (^{1}H, 0.0 ppm) and $CDCl_3$ (^{13}C, 77.16 ppm). The coupling constant *J* is given in Hz. In the ^{1}H NMR spectra, the following abbreviations are used to describe the peak pattern: s (singlet), d (doublet), dd (doublet of doublet), t (triplet), and m (multiplet). Acidic impurities in $CDCl_3$ and $CHCl_3$ were removed by treatment with anhydrous K_2CO_3. IR spectra were recorded on a Perkin-Elmer spectrum 100 spectrometer with an ATR sampling accessory. UV-visible spectra were recorded on a Perkin-Elmer Lambda 25 spectrometer using standard 10 mm quartz cells. High resolution mass analyses were performed at the "Centre Régional de Mesures Physiques de l'Ouest" (CRMPO, University of Rennes 1) using a Bruker MicroTOFQ II apparatus. Column chromatographies were performed using silica gel

Acros SI 60 (60–200 mesh ASTM). Thin-layer chromatography (TLC) was carried out on EMD Silica Gel 60 F_{254} (Merck) or EMD aluminum oxide 150 F_{254} (neutral) plates that were visualized with 365 nm UV light.

4.2. Cyclic voltammetry experimental details

The electrochemical studies were performed with a home-made 3-electrode cell (WE: carbon disk, RE: Ag wire, CE: Pt wire). Decamethylferrocene was added as an internal reference at the end of each experiment; all the potential are quoted against the decamethylferrocenium-decamethylferrocene couple. The potential of the cell was controlled by a µ-AUTOLAB III potentiostat monitored by the GPES software (Metrohm). The supporting salt $[NBu_4][PF_6]$ (Aldrich) was used without further purification.

4.3. Computational details

DFT geometry optimizations were carried out using the Gaussian 09 package,[60] employing the PBE0 functional,[61-63] together with the D3 version of Grimme's empirical dispersion (Becke-Johnson damping)[64] and using the Def2-TZVP basis set.[65] Solvent (chloroform) effects have been taken into account using the PCM model.[66-67] All stationary points were fully characterized via analytical frequency calculations as true minima (no imaginary values). The composition of the Kohn-Sham orbitals was calculated using the AOMix program.[68] The graphical GaussView interface was used.[69] The UV-visible transitions were calculated by means of TD-DFT calculations on the optimized geometries with the CAM-B3LYP functional[70] which is more appropriate than PBE0 for computing charge-transfer excitation energies. Only singlet-singlet transitions have been taken into account. Only the transitions with non-negligible oscillator strengths are discussed in the paper. The TD-DFT simulated UV-vis spectra were performed using the SWizard program.[71-72] Static and frequency-dependent electronic hyperpolarizabilities were obtained at the TDDFT level

through the coupled-perturbed Kohn-Sham procedure[73-74] using the wB97XD functional[75] with the same basis set as above. Dynamic hyperpolarizabilities were computed assuming a laser wavelength of 1907 nm ($\hbar\omega$ = 0.023896 a.u.) for the SHG [$\beta(-2\omega; \omega, \omega)$] NLO processes. The geometries obtained from DFT calculations were used to perform natural atomic charge analysis with the NBO 5.0 program.[76]

4.4. Synthesis of compound 1

In a round-bottomed flask of 100 mL, 153 mg of 1-[(2,6-diphenyl-4*H*-pyran-4-ylidene) methyl]-1'-formyl-ferrocene **7**[50] (334 µmol, 1 eq), 20 mL of NaOH 5M, 10 drops of aliquat 336 and 41 mg of 4-methylpyrimidine (435 mmol, 1.3 eq) were introduced in this order. The resulting mixture was strongly stirred and refluxed for 4h. The aqueous phase was removed with Pasteur pipette and the solid was washed with water and filtered over silica gel with ethyl acetate. The solvent was removed under reduced pressure and the raw material was purified by column chromatography over silica gel (ethyl acetate) to give compound **1** as a red solid in 46% yield (82 mg, 154 µmol). Mp: 144-145°C; NMR (δ (ppm), $CDCl_3$): ^{1}H (300 MHz): 8.88 (s, 1H), 8.26 (d, $^3J_{HH}$ = 5.3 Hz, 1H), 7.72 (t, $^3J_{HH}$ = 1.8 Hz, 1H), 7.70 (t, $^3J_{HH}$ = 1.3 Hz, 1H), 7.63 (t, $^3J_{HH}$ = 1.7 Hz, 1H), 7.61 (t, $^3J_{HH}$ = 1.6 Hz, 1H), 7.57 (d, $^3J_{HH}$ = 15.8 Hz, 1H), 7.47 – 7.35 (m, 6H), 6.99 (d, $^3J_{HH}$ = 5.2 Hz, 1H), 6.73 (d, $^4J_{HH}$ = 1.4 Hz, 1H), 6.51 (d, $^3J_{HH}$ = 15.8 Hz, 1H), 6.09 (d, $^4J_{HH}$ = 1.4 Hz, 1H), 5.34 (s, 1H), 4.53 (t, $^3J_{HH}$ = 1.8 Hz, 2H), 4.42 (t, $^3J_{HH}$ = 1.8 Hz, 2H), 4.40 (t, $^3J_{HH}$ = 1.7 Hz, 2H), 4.26 (t, $^3J_{HH}$ = 1.7 Hz, 2H); ^{13}C{^{1}H} (75 MHz): 162.5, 158.7, 156.8, 151.6, 149.2, 136.9, 133.7, 133.3, 129.2, 128.9, 128.7, 128.7, 127.8, 124.7, 124.2, 123.3, 117.6, 110.2, 108.5, 102.9, 85.8, 81.6, 71.3, 69.7, 69.4, 69.3; IR (ATR, cm^{-1}): 3028, 1654, 1624, 1567, 1493, 1446, 1382, 1281, 1026, 945, 929, 837, 818, 762, 690; HRMS (ESI): m/z, calculated for $[M+H]^+$ ($C_{34}H_{27}N_2O^{56}Fe$): 535.1467, found: 535.1467, $[M+Na]^+$ ($C_{34}H_{26}N_2ONa^{56}Fe$): 557.1287, found: 557.1286

4.5. Synthesis of compound 2

A mixture of compound **1** (100 mg, 187 µmol) and methyl iodide (5 mL) was refluxed for 20h. The methyl iodide was evaporated under vacuum and the residue was analysed without further purification. The compound **2** was obtained as a red powder in 95% yield (120 mg, 178 µmol). Mp: 154-155°C; NMR (δ (ppm), CD_2Cl_2): ^{1}H (300 MHz): 8.62 (s, 1H), 8.54 (d, $^3J_{HH}$ = 6.7 Hz, 1H), 7.89 (d, $^3J_{HH}$ = 15.1 Hz, 1H), 7.76 (d, $^3J_{HH}$ = 7.1 Hz, 2H), 7.69 (d, $^3J_{HH}$ = 7.6 Hz, 2H), 7.58 – 7.48 (m, 4H), 7.45 (d, $^3J_{HH}$ = 7.8 Hz, 2H), 7.37 – 7.30 (m, 1H), 6.55 (s, 1H), 6.36 (d, $^3J_{HH}$ = 15.1 Hz, 1H), 6.06 (s, 1H), 5.17 (s, 1H), 4.74 (s, 4H), 4.57 (s, 2H), 4.25 (s, 2H), 3.47 (s, 3H); ^{13}C{^{1}H} (75 MHz): 167.6, 152.5, 152.1, 150.8, 149.5, 149.1, 133.7, 133.2, 130.4, 130.1, 129.8, 128.7, 125.4, 124.5, 120.3, 118.4, 109.9, 108.9, 103.4, 89.5, 81.8, 75.4, 72.0, 71.4, 71.1, 44.4 (some carbon atoms are not observed); IR (ATR, cm^{-1}): 3411, 2923, 1980, 1653, 1575, 1468, 1431, 1279, 1195, 1026, 817, 764, 691; HRMS (ESI): m/z, calculated for M^+ ($C_{35}H_{29}N_2O^{56}Fe$): 549.1624, found: 549.1629

4.6. Synthesis of compound 4

A mixture of compound **3** (600 mg, 1.71 mmol) and methyl iodide (5 mL) was refluxed for 2h. The solvent was evaporated under vacuum and the residue was analysed without further purification. The compound **4** was obtained as a dark blue solid in 96% yield (809 mg, 1.64 mmol). Mp: 164-165°C; NMR (δ (ppm), DMSO-d_8): ^{1}H (300 MHz): 9.08 (s, 1H), 8.69 – 8.60 (m, 2H), 8.15 – 8.12 (m, 2H), 8.01 – 7.99 (m, 3H), 7.79 (s, 1H), 7.62 – 7.57 (m, 6H), 7.26 (s, 1H), 6.52 (d, $^3J_{HH}$ = Hz, 1H), 6.21 (d, $^3J_{HH}$ = Hz, 1H), 3.98 (s, 3H); ^{13}C{^{1}H} (75 MHz): 166.6, 155.6, 155.4, 147.5, 143.8, 143.7, 131.4, 131.1, 130.9, 130.8, 129.1, 125.7, 125.2, 120.4, 115.4, 109.3, 103.7, 42.7 (some carbon atoms are not observed); IR (ATR, cm^{-1}): 3430, 3038, 2922, 2161, 1636, 1517, 1491, 1421, 1245, 1198, 1156, 941, 759, 672; HRMS (ESI): m/z, calculated for C^+ ($C_{25}H_{21}N_2O$): 365.1648, found: 365.1652

4.7. Synthesis of compound 6

A mixture of compound **5**[19] (100 mg, 345 µmol) and methyl iodide (5 mL) was refluxed for 20h. The methyl iodide was evaporated under vacuum and the residue was analysed without further purification. The compound **6** was obtained as a dark red powder in 97% yield (144 mg, 334 µmol). Mp: 186-187°C; NMR (δ (ppm), CD_2Cl_2): ^{1}H (300 MHz): 9.03 (d, $^3J_{HH}$ = 1.2 Hz, 1H), 8.57 (d, $^3J_{HH}$ = 5.3 Hz, 1H), 7.74 (d, $^3J_{HH}$ = 15.8 Hz, 1H), 7.21 (dd, J = 5.3, 1.4 Hz, 1H), 6.66 (d, $^3J_{HH}$ = 15.8 Hz, 1H), 4.58 (t, $^3J_{HH}$ = 1.7 Hz, 2H), 4.42 (t, $^3J_{HH}$ = 1.9 Hz, 2H), 4.16 (s, 5H), 1.73 (s, 3H); ^{13}C{^{1}H} (75 MHz): 163.1, 159.3, 157.5, 138.4, 123.3, 118.3, 81.2, 71.4, 71.1, 70.1, 68.8; NMR (δ (ppm), DMSO-d_8): ^{1}H (300 MHz): 9.37 (s, 1H), 8.93 (d, $^3J_{HH}$ = 6.5 Hz, 1H), 8.27 (d, $^3J_{HH}$ = 15.5 Hz, 1H), 7.96 (d, $^3J_{HH}$ = 6.4 Hz, 1H), 7.04 (d, $^3J_{HH}$ = 15.5 Hz, 1H), 4.89 (d, $^3J_{HH}$ = 1.7 Hz, 2H), 4.73 (d, $^3J_{HH}$ = 1.7 Hz, 2H), 4.24 (s, 5H), 4.06 (s, 3H); ^{13}C{^{1}H} (75 MHz): 166.3, 153.2, 150.3, 149.2, 119.8, 117.6, 78.9, 72.8, 70.0, 69.7, 43.4; IR (ATR, cm^{-1}): 3075, 1640, 1585, 1542, 1471, 1440, 1191, 1175, 866, 821, 808, 755; HRMS (ESI): m/z, calculated for M^+ ($C_{17}H_{17}N_2{}^{56}Fe$): 305.0736, found: 305.0738

Appendix A . Supplementary data

Supplementary data related to this article can be found at ....

References

1 P. N. Prasad and D. J. Williams, *Introduction to nonlinear optical effects in molecules and polymers*, Wiley, New York, 1991.

2 P. N. Prasad, *Nonlinear Optical Properties of Organic Materials*, Plenum, New York, 1991.

3 P. N. Prasad, *Nanophotonics*, Wiley, Hoboken, NJ, 2004.

4 J. Xu, S. Semin, D. Nietzialek, P. H. J. Kouwer, E. Fron, E. Coutino, M. Savoini, Y.

Li, J. Hofkens, H. Uji-I, D. Beljone, T. Rasing and A. E. Rowan, *Adv. Mater.* 2013, **25**, 2084-2089.

5 R. W. Boyd, *Nonlinear optics*, Academic Press, Amsterdam ; Boston, 3rd ed., 2008.

6 K. Clays and B. J. Coe, *Chem. Mater.*, 2003, **15**, 642–648.

7 M. O. Senge, M. Fazekas, E. G. A. Notaras, W. J. Blau, M. Zawadzka, O. B. Locos and E. M. Ni Mhuircheartaigh, *Adv. Mater.*, 2007, **19**, 2737–2774.

8 C. Hu, Z. Chen, H. Xiao, Z. Zhen, X. Liu and S. Bo, *J. Mater. Chem. C*, 2017, **5**, 5111–5118.

9 C. Ouyang, J. Liu, Q. Liu, Y. Li, D. Yan, Q. Wang, M. Guo and A. Cao, *ACS Appl. Mater. Interfaces*, 2017, **9**, 10366–10370.

10 F. Liu, H. Wang, Y. Yang, H. Xu, D. Yang, S. Bo, J. Liu, Z. Zhen, X. Liu and L. Qiu, *Dyes Pigments*, 2015, **114**, 196–203.

11 M. Li, Y. Li, H. Zhang, S. Wang, Y. Ao and Z. Cui, *J. Mater. Chem. C*, 2017, **5**, 4111–4122.

12 H. Ma, A. k.-Y. Jen and L. r. Dalton, *Adv. Mater.*, 2002, **14**, 1339–1365.

13 J. Kulhánek, F. Bureš, W. Kuznik, I. V. Kityk, T. Mikysek and A. Růžička, *Chem. – Asian J.*, 2013, **8**, 465–475.

14 R. M. El-Shishtawy, F. Borbone, Z. M. Al-amshany, A. Tuzi, A. Barsella, A. M. Asiri and A. Roviello, *Dyes Pigments*, 2013, **96**, 45–51.

15 J. Liu, W. Gao, I. V. Kityk, X. Liu and Z. Zhen, *Dyes Pigments*, 2015, **122**, 74–84.

16 F. Bureš, *RSC Adv.*, 2014, **4**, 58826–58851.

17 B. J. Coe, *Acc. Chem. Res.*, 2006, **39**, 383–393.

18 I. D. L. Albert, T. J. Marks and M. A. Ratner, *J. Am. Chem. Soc.*, 1997, **119**, 6575–6582.

19 S. Achelle, A. Barsella, C. Baudequin, B. Caro and F. Robin-Le Guen, *J. Org. Chem.*, 2012, **77**, 4087–4096.

20 S. Achelle, S. Kahlal, A. Barsella, J.-Y. Saillard, X. Che, J. Vallet, F. Bureš, B. Caro and F. Robin-Le Guen, *Dyes Pigments*, 2015, **113**, 562–570.

21 S. Achelle, A. Barsella, B. Caro and F. Robin-Le Guen, *RSC Adv.*, 2015, **5**, 39218–39227.

22 S. Achelle, J.-P. Malval, S. Aloïse, A. Barsella, A. Spangenberg, L. Mager, H. Akdas-Kilig, J.-L. Fillaut, B. Caro and F. Robin-Le Guen, *ChemPhysChem*, 2013, **14**, 2725–2736.

23 R. J. Durand, S. Gauthier, S. Achelle, S. Kahlal, J.-Y. Saillard, A. Barsella, L. Wojcik, N. L. Poul and F. Robin-Le Guen, *Dalton Trans.*, 2017, **46**, 3059–3069.

24 R. J. Durand, S. Gauthier, S. Achelle, T. Groizard, S. Kahlal, J.-Y. Saillard, A. Barsella, N. Le Poul and F. Robin-Le Guen, *Dalton Trans.* doi: 10.1039/C8DT00093J

25 N. Faux, F. Robin-Le Guen, P. Le Poul, B. Caro, K. Nakatani, E. Ishow and S. Golhen, *Eur. J. Inorg. Chem.*, 2006, 3489–3497.

26 S. Gauthier, N. Vologdin, S. Achelle, A. Barsella, B. Caro and F. Robin-Le Guen, *Tetrahedron*, 2013, **69**, 8392–8399.

27 P. Solanke, S. Achelle, N. Cabon, O. Pytela, A. Barsella, B. Caro, F. Robin-Le Guen, J. Podlesný, M. Klikar and F. Bureš, *Dyes Pigments*, 2016, **134**, 129–138.

28 A. I. Aranda, S. Achelle, F. Hammerer, F. Mahuteau-Betzer and M.-P. Teulade-

Fichou, *Dyes Pigments*, 2012, **95**, 400–407.

29 R. Andreu, E. Galán, J. Garín, V. Herrero, E. Lacarra, J. Orduna, R. Alicante and B. Villacampa, *J. Org. Chem.*, 2010, **75**, 1684–1692.

30 R. Andreu, E. Galán, J. Orduna, B. Villacampa, R. Alicante, J. T. L. Navarrete, J. Casado and J. Garín, *Chem. – Eur. J.*, 2011, **17**, 826–838.

31 A. B. Marco, P. M. Burrezo, L. Mosteo, S. Franco, J. Garín, J. Orduna, B. E. Diosdado, B. Villacampa, J. T. L. Navarrete, J. Casado and R. Andreu, *RSC Adv.*, 2015, **5**, 231–242.

32 C. Moreno-Yruela, J. Garín, J. Orduna, S. Franco, E. Quintero, J. T. López Navarrete, B. E. Diosdado, B. Villacampa, J. Casado and R. Andreu, *J. Org. Chem.*, 2015, **80**, 12115–12128.

33 S. Kaur, M. Kaur, P. Kaur, K. Clays and K. Singh, *Coord. Chem. Rev.*, 2017, **343**, 185–219.

34 B. J. Coe, *Coord. Chem. Rev.*, 2013, **257**, 1438–1458.

35 K. Senthilkumar, K. Thirumoorthy, C. Dragonetti, D. Marinotto, S. Righetto, A. Colombo, M. Haukka and N. Palanisami, *Dalton Trans.*, 2016, **45**, 11939–11943.

36 M. Zaarour, A. Singh, C. Latouche, J. A. G. Williams, I. Ledoux-Rak, J. Zyss, A. Boucekkine, H. Le Bozec, V. Guerchais, C. Dragonetti, A. Colombo, D. Roberto and A. Valore, *Inorg. Chem.*, 2013, **52**, 7987–7994.

37 P. Kaur, M. Kaur, G. Depotter, S. V. Cleuvenbergen, I. Asselberghs, K. Clays and K. Singh, *J. Mater. Chem.*, 2012, **22**, 10597–10608.

38 S. Salman, J.-L. Brédas, S. R. Marder, V. Coropceanu and S. Barlow,

Organometallics, 2013, **32**, 6061–6068.

39 D. Astruc, *Eur. J. Inorg. Chem.*, 2017, 6–29.

40 I. Baumgardt and H. Butenschön, *Eur. J. Org. Chem.*, 2010, 1076–1087.

41 C. Engtrakul and L. R. Sita, *Organometallics*, 2008, **27**, 927–937.

42 T.-Y. Dong, K. Chen, M.-C. Lin and L. Lee, *Organometallics*, 2005, **24**, 4198–4206.

43 H.-Q. Wu, H.-L. Xu, S.-L. Sun and Z.-M. Su, *Dyes Pigments*, 2014, **106**, 7–13.

44 J. Zyss, I. Ledoux, S. Volkov, V. Chernyak, S. Mukamel, G. P. Bartholomew and G. C. Bazan, *J. Am. Chem. Soc.*, 2000, **122**, 11956–11962.

45 A. Takai, T. Yasuda, T. Ishizuka, T. Kojima and M. Takeuchi, *Angew. Chem. Int. Ed.*, 2013, **52**, 9167–9171.

46 N. Kraußе and H. Butenschön, *Eur. J. Org. Chem.*, 2014, 6686–6695.

47 S. Ø. Scottwell, A. B. S. Elliott, K. J. Shaffer, A. Nafady, C. J. McAdam, K. C. Gordon and J. D. Crowley, *Chem. Commun.*, 2015, **51**, 8161–8164.

48 J. D. Crowley, I. M. Steele and B. Bosnich, *Chem. – Eur. J.*, 2006, **12**, 8935–8951.

49 N. Vologdin, S. Gauthier, S. Achelle, B. Caro and F. Robin-Le Guen, *Lett. Org. Chem.*, 2014, **11**, 606–614.

50 F. Ba, F. Robin-Le Guen, N. Cabon, P. Le Poul, S. Golhen, N. Le Poul and B. Caro, *J. Organomet. Chem.*, 2010, **695**, 235–243.

51 S. Achelle, S. Kahlal, J.-Y. Saillard, N. Cabon, B. Caro and F. Robin-Le Guen, *Tetrahedron*, 2014, **70**, 2804–2815.

52 F. Ba, N. Cabon, P. Le Poul, S. Kahlal, J.-Y. Saillard, N. Le Poul, S. Golhen, B. Caro

and F. Robin-Le Guen, *New J. Chem.*, 2013, **37**, 2066.

53 L. Wojcik, F. Michaud, S. Gauthier, N. Cabon, P. Le Poul, F. Gloaguen and N. Le Poul, *J. Org. Chem.*, 2017, **82**, 12395–12405.

54 L. E. R. Buckley, B. J. Coe, D. Rusanova, S. Sánchez, M. Jirásek, V. D. Joshi, J. Vávra, D. Khobragade, L. Pospíšil, Š. Ramešová, I. Císařová, D. Šaman, R. Pohl, K. Clays, N. V. Steerteghem, B. S. Brunschwig and F. Teplý, *Dalton Trans.*, 2017, **46**, 1052–1064.

55 G. Ulrich, A. Barsella, A. Boeglin, S. Niu, and R. Ziessel, R. *ChemPhysChem.*, 2014, **15**, 2693-2700.

56 K. D. Singer, and A. F. Garito, *J. Phys. Chem.* 1981, **75**, 3572-3580.

57 B. F. Levine, and C. G. Bethea, *Appl. Phys. Lett.* 1974, **24**, 445-447.

58 I. Ledoux, and J. Zyss, *Chem. Phys.* 1982, **73**, 203-213.

59 T. Thami, P. Bassoul, M. A. Petit, J. Simon, A. Fort, M. Barzoukas, and A. Villaeys, *J. Am. Chem. Soc.* 1992, **114**, 915-921.

60 Gaussian 09, Revision D.01, M. J. Frisch, G. W. Trucks, H. B. Schlegel, G. E. Scuseria, M. A. Robb, J. R. Cheeseman, G. Scalmani, V. Barone, B. Mennucci, G. A. Petersson, H. Nakatsuji, M. Caricato, X. Li, H. P. Hratchian, A. F. Izmaylov, J. Bloino, G. Zheng, J. L. Sonnenberg, M. Hada, M. Ehara, K. Toyota, R. Fukuda, J. Hasegawa, M. Ishida, T. Nakajima, Y. Honda, O. Kitao, H. Nakai, T. Vreven, J. A. Montgomery, Jr., J. E. Peralta, F. Ogliaro, M. Bearpark, J. J. Heyd, E. Brothers, K. N. Kudin, V. N. Staroverov, T. Keith, R. Kobayashi, J. Normand, K. Raghavachari, A. Rendell, J. C. Burant, S. S. Iyengar, J. Tomasi, M. Cossi, N. Rega, J. M. Millam, M. Klene, J. E. Knox, J. B. Cross, V. Bakken, C. Adamo, J. Jaramillo, R. Gomperts, R. E. Stratmann, O. Yazyev, A. J. Austin, R. Cammi, C. Pomelli, J. W. Ochterski, R. L. Martin, K. Morokuma, V. G. Zakrzewski, G. A. Voth, P.

Salvador, J. J. Dannenberg, S. Dapprich, A. D. Daniels, O. Farkas, J. B. Foresman, J. V. Ortiz, J. Cioslowski, and D. J. Fox, Gaussian, Inc., Wallingford CT, 2013.

61 J. P. Perdew, K. Burke, and M. Ernzerhof, *Phys. Rev. Lett.*1996, **77**, 3865-3868.

62 J. P. Perdew, K. Burke, and M. Ernzerhof, *Phys. Rev. Lett.* 1997, **78,** 1396-1396.

63 C. Adamo and V. Barone, *J. Chem. Phys.*1999, **110,** 6158-6169.

64 S. Grimme, S. Ehrlich and L. Goerigk, *J. Comp. Chem*. 2011, **32**, 1456-1465.

65 F. Weigend and R. Ahlrichs, *Phys. Chem. Chem. Phy*s. 2005, **7**, 3297-3305.

66 M. Cossi, V. Barone, R. Cammi, and J. Tomasi, *Chem. Phys. Lett.* 1996, **255**, 327-335.

67 V. Barone, M. Cossi, and J. Tomasi, *J. Chem. Phys.* 1997, **107**, 3210-3221.

68 S. I. Gorelsky, AOMix: program for molecular orbital analysis, *York University, Toronto*, 1997.

69 R. Dennington, T. Keith, J. Millam, K. Eppinnett, W. L. Hovell, and R. Gilliland, GaussView, 2009.

70 T. Yanai, D. Tew, and N. Handy, *Chem. Phys. Lett.* 2004, **393**, 51-57.

71 S. I. Gorelsky, *SWizard program*, http://www.sg-chem.net/, University of Ottawa, Ottawa, Canada, 2013.

72 S. I. Gorelsky and A. B. P. Lever, *J. Organomet. Chem.* 2001, **635**, 187-196.

73 H. Sekino and R. J. Bartlett, *J. Chem.Phys*. 1986, **85**, 976-989.

74 J. E. Rice and N. C. Handy, *Int. J. Quantum Chem*. 1992, **43**, 91-118.

75 J. D. Chai and M. Head-Gordon, *Phys. Chem. Chem. Phys.* 2008, **10**, 6615-6620.

76 E. D. Glendening, J. K. Badenhoop, A. E. Reed, J. E. Carpenter, J. A. Bohmann, C. M. Morales and F. Weinhold, **2001**, NBO 5.0; Theoretical Chemistry Institute, University of Wisconsin, Madison, WI, http://www.chem.wisc.edu/~nbo5.

Highlights

- Ferrocene unit was incorporated in the π-conjugated linker or D-π-A compounds.
- Intramolecular charge transfer through ferrocene moiety was studied.
- Electrochemical and photophysical properties were compared with all organic analogues.
- The ferrocene unit limits charge transfert from donor to acceptor.